Magn Reson Med Sci 2025; 24; 66–77
doi:10.2463/mrms.mp.2023-0102 Published Online: November 10, 2023

MAJOR PAPER

# Evaluating Reproducibility of the ADC and Distortion in Diffusion-weighted Imaging (DWI) with Reverse Encoding Distortion Correction (RDC)

Hitomi Numamoto[1], Koji Fujimoto[1*], Kanae Kawai Miyake[1], Yasutaka Fushimi[2], Sachi Okuchi[2], Rimika Imai[3], Hiroki Kondo[3], Tsuneo Saga[1], and Yuji Nakamoto[2]

**Purpose:** To compare image distortion and reproducibility of quantitative values between reverse encoding distortion correction (RDC) diffusion-weighted imaging (DWI) and conventional DWI techniques in a phantom study and in healthy volunteers.

**Methods:** This prospective study was conducted with the approval of our institutional review board. Written informed consent was obtained from each participant. RDC-DWIs were created from images obtained at 3T in three orthogonal directions in a phantom and in 10 participants (mean age, 70.9 years; age range, 63–83 years). Images without distortion correction (noDC-DWI) and those corrected with B0 (B0c-DWI) were also created. To evaluate distortion, coefficients of variation were calculated for each voxel and ROIs were placed at four levels of the brain. To evaluate the reproducibility of apparent diffusion coefficient (ADC) measurements, intra- and inter-scan variability ($\%CV_{ADC}$) were calculated from repeated scans of the phantom. Analysis was performed using Wilcoxon signed-rank test with Bonferroni correction, and $P < 0.05$ was considered statistically significant.

**Results:** In the phantom, distortion was less in RDC-DWI than in B0c-DWI ($P < 0.006$), and was less in B0c-DWI than in noDC-DWI ($P < 0.006$). Intra-scan $\%CV_{ADC}$ was within 1.30%, and inter-scan $\%CV_{ADC}$ was within 2.99%. In the volunteers, distortion was less in RDC-DWI than in B0c-DWI in three of four locations ($P < 0.006$), and was less in B0c-DWI than in noDC-DWI ($P < 0.006$). At the middle cerebellar peduncle, distortion was less in RDC-DWI than in noDC-DWI ($P < 0.006$), and was less in noDC-DWI than in B0c-DWI ($P < 0.0177$).

**Conclusion:** In both the phantom and in volunteers, distortion was the least in RDC-DWI than in B0c-DWI and noDC-DWI.

**Keywords:** *diffusion magnetic resonance imaging, distortion correction, echo-planar imaging*

## Introduction

Diffusion-weighted imaging (DWI) is a widely used MR imaging technique in clinical practice, for which spin-echo-based single-shot echo-planar imaging (SS-EPI) is often used. However, EPI is seriously disadvantaged by image distortion caused by B0 field inhomogeneity and eddy currents.[1]

A number of post-processing methods have been proposed to correct susceptibility-induced geometric distortion, most of which have been developed and applied for brain imaging. These include B0 field mapping,[2] registration approaches,[3] use of a reverse polarity gradient (RPG),[4] and a deep-learning-based method.[5] Historically, in 1992, Chang et al. proposed a method for correcting image distortion in the spin-echo sequence that used a pair of images with altered phase-encoding gradients.[6] In 1994, Bowtell et al. applied this technique to EPI.[7] Andersson et al. extended the concept in 2003 to achieve diffusion-tensor maps with very little distortion (TOPUP).[4] They subsequently presented a model-based method for reducing the effects of eddy-current-induced distortion in 2002.[8] Several methods have

[1]Department of Advanced Imaging in Medical Magnetic Resonance, Graduate School of Medicine, Kyoto University, Kyoto, Kyoto, Japan
[2]Department of Diagnostic Imaging and Nuclear Medicine, Graduate School of Medicine, Kyoto University, Kyoto, Kyoto, Japan
[3]Canon Medical Systems Corporation, Otawara, Tochigi, Japan
*Corresponding author: Department of Advanced Imaging in Medical Magnetic Resonance, Kyoto University Graduate School of Medicine, 54 Shogoin Kawaharacho, Sakyoku, Kyoto, Kyoto 606-8507, Japan. Phone: +81-75-751-3760, E-mail: kfb@kuhp.kyoto-u.ac.jp



Received: August 7, 2023 | Accepted: October 2, 2023

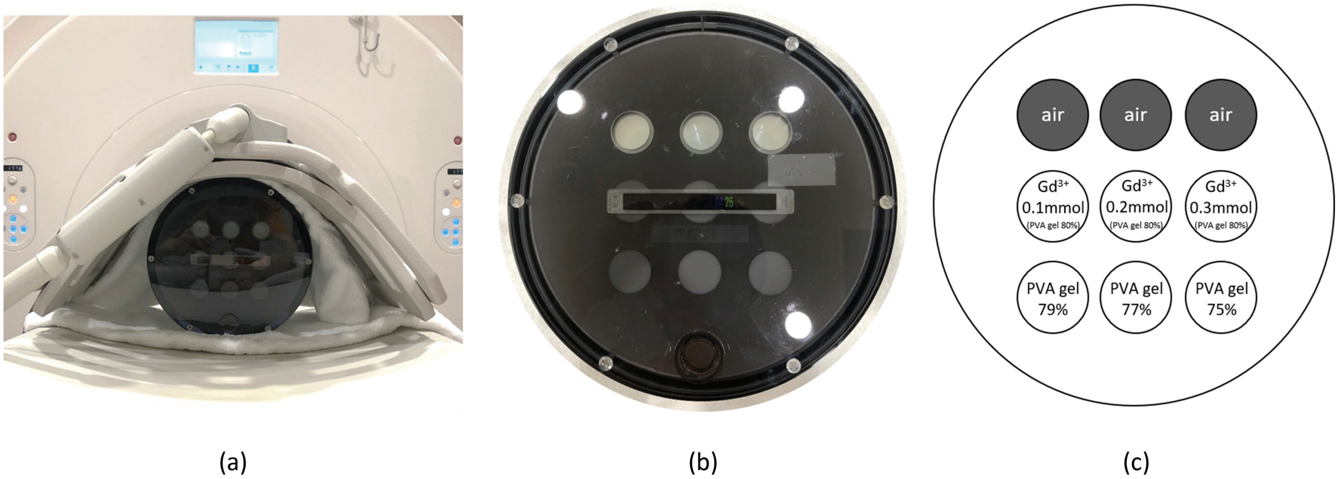


**Fig. 1** Experimental setup for the phantom study. The phantom was positioned on the table such that all nine circular tubes were in the same axial plane (**a**). A 16-channel body array coil is placed around the phantom (**a**). The three circles in the upper row correspond to empty slots for user-prepared phantom tubes, which in this case were kept empty (**b**, **c**). PVA gel, polyvinyl alcohol gel.

a faster reconstruction time than TOPUP, including the block-matching method,[9] the diffeomorphic registration-based method (DR-BUDDI)[10], and a technique that uses a fast nonlinear registration procedure (EPIC).[11] Andersson et al. recently proposed an approach to correct for eddy-current-induced and susceptibility-induced distortion in diffusion MRI (FSL eddy).[12] However, these methods cannot be used in clinical practice because they require an off-line post-processing workstation.

A method termed reverse encoding distortion correction (RDC) DWI, which is based on the reversed gradient correction method for EPI imaging[13] with a smoothness in the model[14] and a paired acquisition of the images with diffusion gradients,[15] has recently become available in a clinical scanner. However, the extent of distortion correction and the reproducibility of quantitative values in RDC-DWI have not been thoroughly investigated. The purpose of this study was to compare image distortion among RDC-DWI, DWI with B0 correction only (B0c-DWI), and conventional DWI ([images without distortion correction] noDC-DWI) created from images acquired in a phantom and in healthy volunteers, and to evaluate reproducibility of the quantitative values in the phantom scan data.

## Materials and Methods

### *Experimental setting for the phantom*

Figure 1 shows the setup for the phantom study. We used an MRI phantom (94-401; Motohashi Kasei Kogyo Ltd, Matsudo, Japan) containing three hollow tube slots and six tubes. The hollow tube slots were intentionally kept empty to simulate air spaces in the human body, such as the paranasal sinuses. To evaluate distortion, 10 independent 2D DWI scans were performed in each of three orthogonal directions (axial, coronal, and sagittal). To evaluate the reproducibility of the ADC values, five independent DWI scans were performed consecutively in the axial plane in each of five sessions, which were performed on five consecutive days. For the evaluation of reproducibility, 25 scans were performed in total.

### *Participants*

This prospective study was approved by the local institutional review board and was registered to jRCT (s052200018). The study was performed in accordance with the ethical standards of the Declaration of Helsinki. Ten healthy volunteers (mean age, 70.9 years; age range, 63–83 years; six males, four females) were prospectively enrolled between 14 January 2022 and 13 May 2022. All participants provided written informed consent to participate in this study. The exclusion criterion was poor quality images due to body movement during the MRI data acquisition.

### *Image acquisition*

In both the phantom and the participants, imaging was acquired with a whole-body 3T MRI unit (Vantage Centurian; Canon Medical Systems Corporation, Otawara, Japan). Multi-slice 2D DWI was obtained in the axial, coronal, and sagittal planes using a single-shot SE-EPI sequence with b values of 0 and 1000 s/mm$^2$. The reason we performed three DWI scans (i.e. axial, coronal, and sagittal) was because we wanted to create a distortion map using the method described below. For signal reception, the combination of a 16-channel body array coil and a 32-channel spine array coil was used for the phantom, and a 32-channel head coil was used for the participants. The reason that we had to use body coil for phantom scans was because the phantom was too big to fit in the head coil. Image domain based parallel imaging technique was used, with acceleration

**Table 1** Scan parameters used in both phantom and volunteer studies

| | Phantom | Healthy volunteer |
|---|---|---|
| Coil | 16ch Body and 32ch Spine | 32ch Head |
| TR (msec) | 9000 | 4500 |
| TE (msec) | 65 | 65 |
| Slice thickness (mm) | 3 | 3 |
| Bandwidth (Hz/pixel) | 1563 | 1563 |
| FOV ($cm^2$) | 28.8 × 28.8 | 22 × 22 |
| Matrix | 192 × 192 | 136 × 160 |
| Resolution | 1.5 × 1.5 | 1.7 × 1.4 |
| SPEEDER | 2×, 3× | 3× |
| Scan time (min) | 4:48 | 2:24 |

SPEEDER; acceleration factor.

factors (Acc) of 2 and 3 for the phantom and Acc of 3 for the participants. Table 1 lists the scan parameters in detail. The number of slices was set to 64 to cover the entire volume of the phantom, resulting in a longer TR (9000 msec) for the phantom than for the participants (4500 msec). FOV for the phantom was set to 26 cm, which is larger than the FOV for the volunteer scan (22 cm), because the diameter of the phantom was 22 cm. As for the matrix, we chose parameters such that ROI measurement for the tube was possible, and thus the conditions were different from those for the volunteer imaging.

The number of excitations (NEX) for all scans was 2 (a pair of opposite phase-encoding directions; i.e., forward and reverse directions). The b0 images were scanned once (NEX 1) for each phase encoding direction, and the b1000 images were scanned four times (NEX 4) for each phase encoding direction, with motion probing gradients (MPGs) in three directions.

### *Retrospective reconstruction of DWI*

Both B0 correction and eddy-current correction were applied in the proposed RDC-DWI method. In addition, DWI with B0 correction only (B0c-DWI) and DWI without distortion correction (noDC-DWI) were reconstructed retrospectively from the same raw data (Fig. 2). For RDC-DWI, two b0 images and 24 b1000 images (i.e., NEX 4, three MPG directions, forward and reverse phase encoding directions) were used for each slice. For B0c-DWI, two b0 images (forward and reverse) and 12 b1000 images (forward only) were used for each slice. For noDC-DWI, one b0 image and 12 b1000 images (forward only) were used for each slice. This retrospective reconstruction step was performed in the axial, coronal, and sagittal plane, respectively.

### *Image post-processing to quantify the degree of distortion*

Among a variety of methods to evaluate the degree of distortion, we chose to modify the method of Irfanoglu et al., where they calculated distortion by subtracting distortion-corrected images obtained from AP-PA pair and the LR-RL pair.[16] In their distortion maps, the contours of the brain appear bright due to high standard deviation (SD) values in these areas. In this study, instead, we calculated SD of DWIs obtained in the axial, sagittal, and coronal slice orientations. Figure 3 and supplementary Fig. 1 show the steps in image post-processing for analysis of distortion. Briefly, the three orthogonal DWI volumes of multi-slice 2D images, as we described in the previous section, were reformatted into an axial 1.4 mm isotropic volume. From the three reformatted volumes obtained from the axial (Ar: axial-reformatted), coronal (Cr: coronal-reformatted), and sagittal (Sr: sagittal-reformatted) images, the following images were calculated in a pixel-by-pixel basis based on the formula 1–3 shown below; mean image (M), SD image, and distortion image using coefficient of variation ($CV_{distortion}$). Please note that Ar, Cr, Sr, M, SD, and $CV_{distortion}$ represent image volume, and mathematical operation (multiplication, division, etc.) were performed in a pixel-by-pixel basis. The mean value of $CV_{distortion}$ was obtained for ROIs placed as described below. $CV_{distortion}$ at each voxel is a measure of variation in signal across the original axial, coronal, and sagittal volumes. As increased distortion results in higher SD values at corresponding voxels, we considered that higher $CV_{distortion}$ values would indicate larger degrees of image distortion.[16] The calculation procedure was applied to RDC-DWI, B0c-DWI, and noDC-DWI independently.

$$M = \frac{Ar + Cr + Sr}{3} \tag{1}$$

$$SD = \sqrt{\frac{\left\{(Ar - M)^2 + (Cr - M)^2 + (Sr - M)^2\right\}}{3}} \tag{2}$$

$$CV_{distortion} = 100 \times \frac{SD}{M} \tag{3}$$

In the images of the phantom, a large circular ROI was placed to cover all nine of the tubes (arrowheads in Fig. 4). As described in the previous section, three of the nine tubes contained air. $CV_{distortion}$ values were compared among RDC-DWI, B0c-DWI, and noDC-DWI, and were also compared between Acc of 2 and 3.

In the images of the participants, a ROI was placed at each of the level of the splenium of the corpus callosum, genu of the corpus callosum, optic chiasm, and middle cerebellar peduncle (Fig. 5).

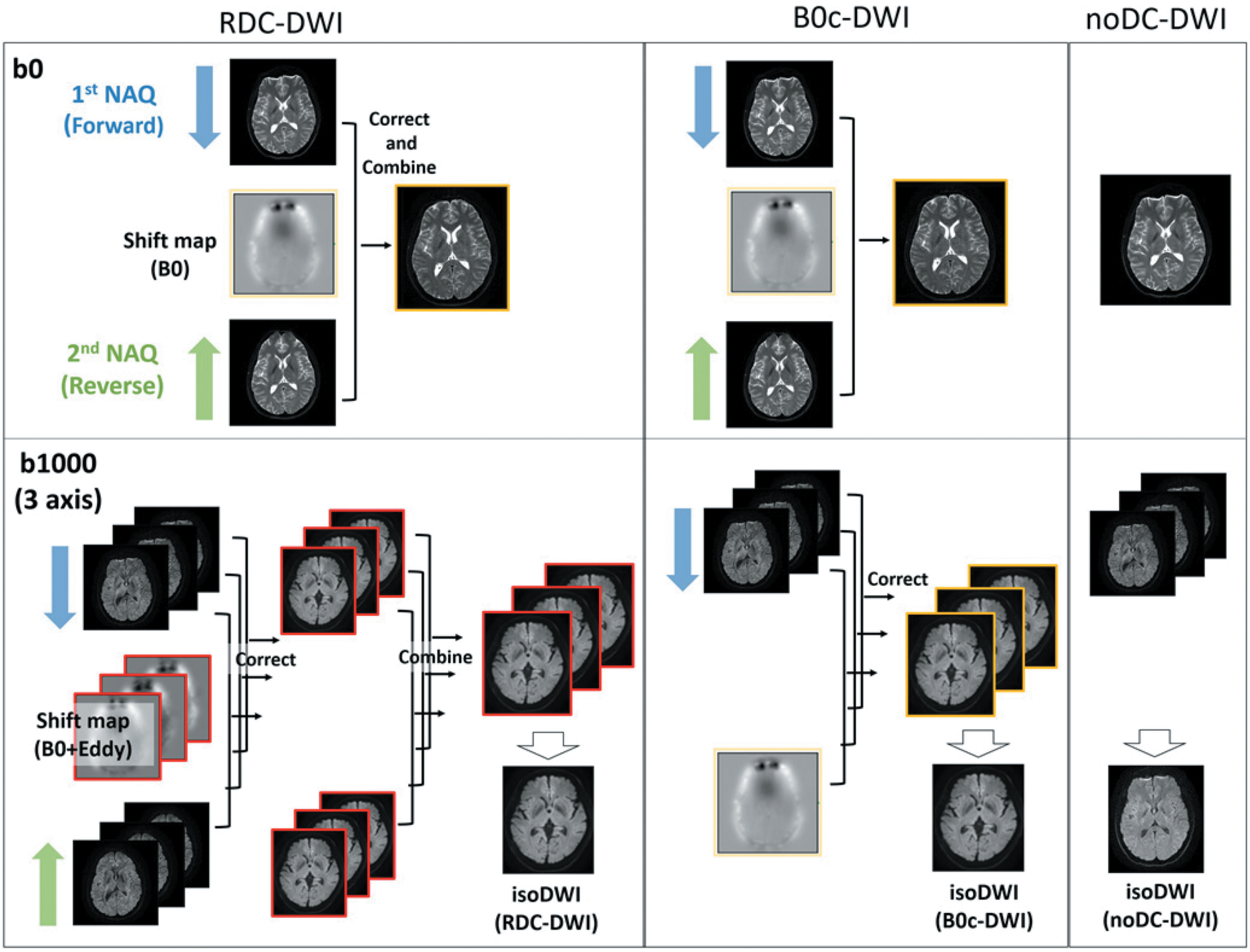


**Fig. 2** Schematic diagram of RDC-DWI (left), B0c-DWI (middle), and noDC-DWI (right). For both RDC-DWI and B0c-DWI, b0 images in forward and reverse directions are used to estimate a B0 shift map with which the b0 images are corrected and combined. For RDC-DWI, the B0 shift map and b1000 images are used to estimate a B0 + MPG shift map used to correct the b1000 images. For B0c-DWI, the B0 shift map was used to correct the b1000 images. No shift map is used for noDC-DWI. DWI in the three MPG directions are combined to obtain isoDWI. B0c, images with B0 correction only; DWI, diffusion-weighted imaging; isoDWI, isotropic diffusion-weighted image; MPG, motion probing gradient; noDC, images without distortion correction; RDC, reverse encoding distortion correction.

### *Statistical method*

As there were 10 samples in both the phantom and volunteer scans, we used a non-parametric test for the paired samples (i.e., Wilcoxon signed-rank test). Bonferroni correction was performed to correct for multiple comparisons, and $P < 0.05$ was considered to indicate a significant difference. All statistical analyses were performed using JMP Pro16.2.0 software (SAS Institute, Cary, NC, USA).

### *Reproducibility analysis for ADC measurement in the phantom*

One of the authors (HN) placed an ROI of diameter 1.5 cm on the tube in the center of the phantom. In this ROI, we obtained 25 data points (5 repetitions × 5 days) for each distortion correction method. For the reproducibility analysis of ADC measurement, we used images with Acc of 2 but not those with Acc of 3, for which we found non-trivial artifacts associated with parallel imaging in the ADC maps.

Three different distortion correction methods were compared using 25 data points of mean ADC value in the ROI. Intra- and inter-scan variability of ADC was measured by calculating the coefficient of variation within the same day (intra-scan $\%CV_{ADC}$) and across different days (inter-scan $\%CV_{ADC}$), respectively.

## Results

### *Distortion in images of the phantom*

Figure 6 shows representative images in the axial, coronal, and sagittal planes for RDC-DWI, B0c-DWI, noDC-DWI for

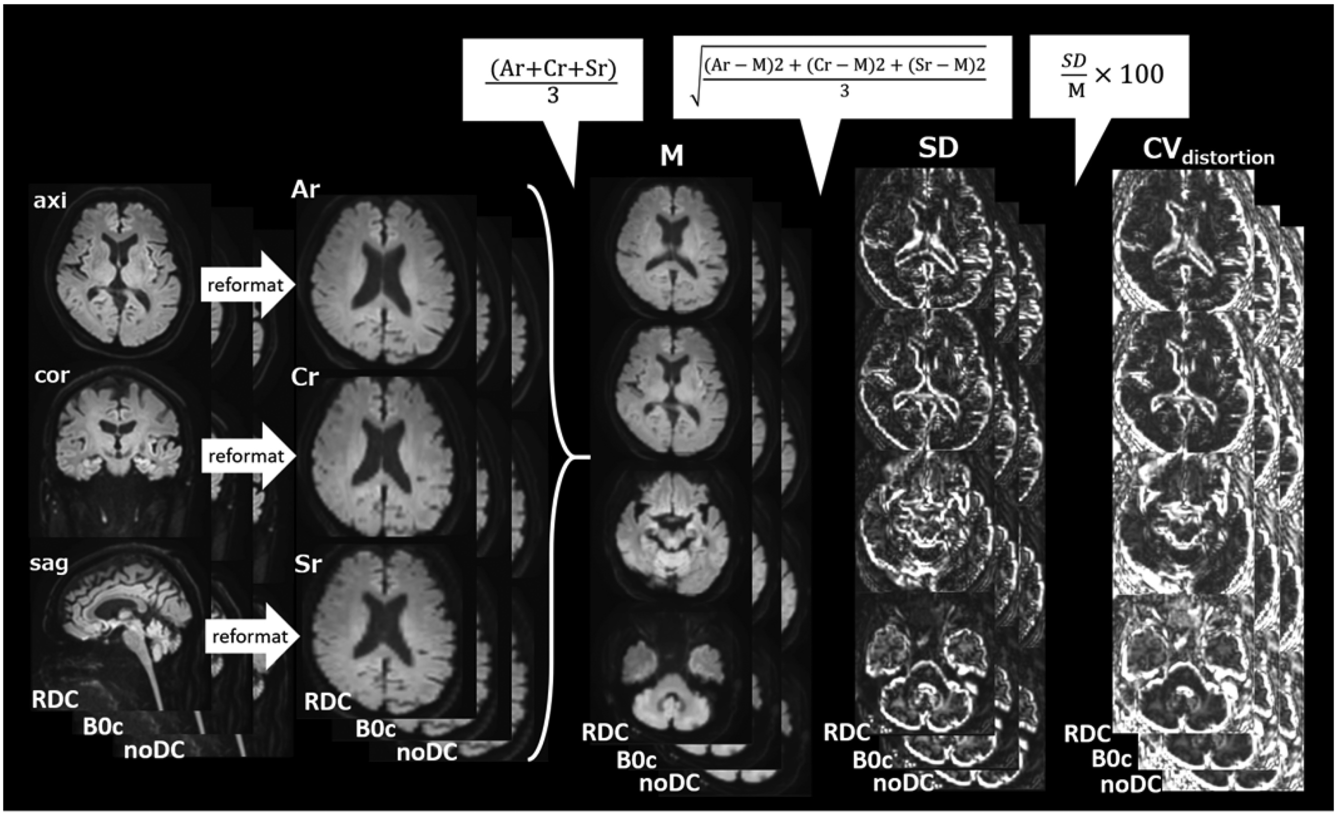


**Fig. 3** Image processing steps for generating $CV_{distortion}$ images. Axial, coronal, and sagittal 2D DWI are first reformatted to axial 1.4 mm-thick images. Images generated from the Ar, Cr, and Sr images are then used to calculate the M images and the SD images using the formulae shown in the figure. Finally, $CV_{distortion}$ images are calculated by dividing SD by M and then multiplied by 100. This process was applied independently to RDC, B0c, and noDC. DWI, diffusion-weighted imaging; Ar, axial; Cr, coronal; Sr, sagittal; M, mean; SD, standard deviation; $CV_{distortion}$, distortion image using coefficient of variation; RDC, reverse encoding distortion correction; B0c, images with B0 correction only; noDC, images without distortion correction.

each acceleration factor in the phantom. Areas of susceptibility artifact are shown with arrows. Susceptibility artifacts are prominent around the empty tubes.

Representative $CV_{distortion}$ maps are shown in Fig. 4. The results of $CV_{distortion}$ in the phantom scans are summarized in Fig. 7. For both Acc values, $CV_{distortion}$ was significantly less in RDC-DWI than in B0c-DWI (Acc 2, $P = 0.006$; Acc 3, $P = 0.006$) and noDC-DWI (Acc 2, $P = 0.006$; Acc 3, $P = 0.006$). Similarly, $CV_{distortion}$ was significantly less in B0c-DWI than in noDC-DWI (Acc 2, $P = 0.006$; Acc 3, $P = 0.006$).

### *ADC in images of the phantom*

Mean ADC value, intra-scan $\%CV_{ADC}$, and inter-scan $\%CV_{ADC}$ of the 25 scans are shown for RDC-DWI (Table 2a), B0c-DWI (Table 2b), and noDC-DWI (Table 2c).

Mean ADC was 2.82% higher in B0c-DWI than in RDC-DWI ($P < 0.0001$), and was 1.91% higher in noDC-DWI than in RDC-DWI ($P < 0.0001$) (statistically significant difference).

There was no significant difference among RDC-DWI, B0c-DWI, and noDC-DWI in terms of intra-scan $\%CV_{ADC}$ or inter-scan $\%CV_{ADC}$ (Fig. 8).

### *Distortion in images of the participants*

No participant was excluded. Distortion was observed inferiorly in the temporal lobes adjacent to the sphenoid sinus, in the right insula, inferiorly in the frontal lobe, and in the suprasellar area in B0c-DWI and noDC-DWI before re-slicing (Fig. 9). In RDC-DWI, distortion was barely noticeable in these regions. In the sagittal images, signal inhomogeneity in the spinal cord was observed in B0c-DWI and noDC-DWI.

Figure 10 shows the $CV_{distortion}$ values for RDC-DWI, B0c-DWI, and noDC-DWI at the four different levels of the brain (splenium of the corpus callosum, genu of the corpus callosum, optic chiasm, and middle cerebellar peduncle). Representative $CV_{distortion}$ maps are shown in Fig. 5. At all locations, $CV_{distortion}$ values were significantly less in RDC-DWI than in B0c-DWI and noDC-DWI ($P < 0.006$). Except for the middle cerebellar peduncle, $CV_{distortion}$ values were significantly less in RDC-DWI than in noDC-DWI ($P < 0.006$); and $CV_{distortion}$ values were significantly less in noDC-DWI than in B0c-DWI ($P < 0.0177$).

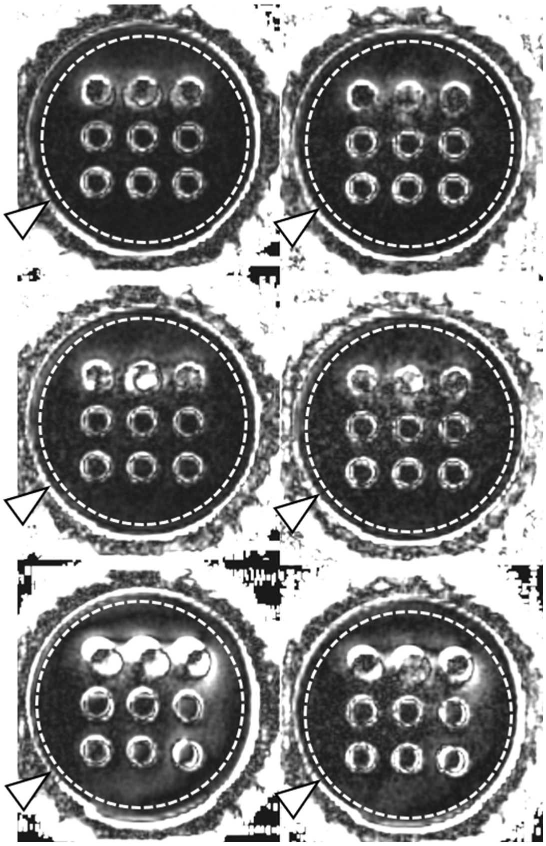


**Fig. 4** $CV_{distortion}$ images calculated from axial, sagittal, and coronal scans for Acc values of 2 (left) and 3 (right). The bright areas around empty tubes indicate high CV, which in this study is interpreted as an area of greater image distortion. ROIs were drawn in images obtained of the phantom to sufficiently cover all nine tubular areas, shown here as dashed circles (arrowheads). B0c, images with B0 correction only; CV, coefficient of variation; $CV_{distortion}$, distortion image using coefficient of variation; DWI, diffusion-weighted imaging; noDC, images without distortion correction; RDC, reverse encoding distortion correction.

## Discussion

In this study, we compared ADC value only in the phantom study. If the difference in the ADC was compared in the relative value (i.e. percentage), mean ADC was 1.91% less in RDC-DWI than in noDC-DWI ($P < 0.001$), and was 2.82% less in RDC-DWI than in B0c-DWI ($P < 0.001$). In other words, mean ADC was the least in RDC-DWI, followed by noDC-DWI and B0c-DWI. If the difference in the ADC was explained in the absolute value, mean ADC was less in RDC-DWI than in B0c-DWI by $0.007–0.07 \times 10^{-3}$ mm/s, and was less in RDC-DWI than in noDC-DWI by $0.006–0.06 \times 10^{-3}$ mm/s. Sjöholm et al.[17] compared ADC values of various normal organs *in vivo* in DWI with and without distortion correction, and found an ADC mean difference of $0.010 \times 10^{-3}$ mm/s at the cerebellum at 3T, although our results in the phantom cannot be compared with these previously obtained results *in vivo*. Nevertheless, the difference in the ADC map seen in our study may not significantly affect in the clinical context.

Intra-scan variability ($\%CV_{ADC}$) was within 1.30% and inter-scan variability ($\%CV_{ADC}$) was within 2.99%. Ideally, evaluation of variability should be performed using a dedicated diffusion phantom, which is capable of dealing with thermal control issues.[18] However, our experiment was performed using a more commonly available phantom at room temperature. Under these conditions, Miquel et al.[19] reported *in vitro* $\%CV_{ADC}$ of 0.5%–1.0% over one day, and 1.3% over 100 days. Similarly, Wang et al.[20] reported *in vitro* intra-scan $\%CV_{ADC}$ of 1.1%, and 2.4% over six months. Although the present intra-scan $\%CV_{ADC}$ and inter-scan $\%CV_{ADC}$ values are comparable with those reported previously by Wang et al., the use of a commercial diffusion phantom remains essential for assessment of the accuracy of ADC.

As a quantitative method to measure, Irfanoglu et al.[16] calculated distortion by subtracting distortion-corrected images obtained from AP-PA pair and the LR-RL pair. In this study, instead, we calculated SD of DWIs obtained in the axial, sagittal, and coronal slice

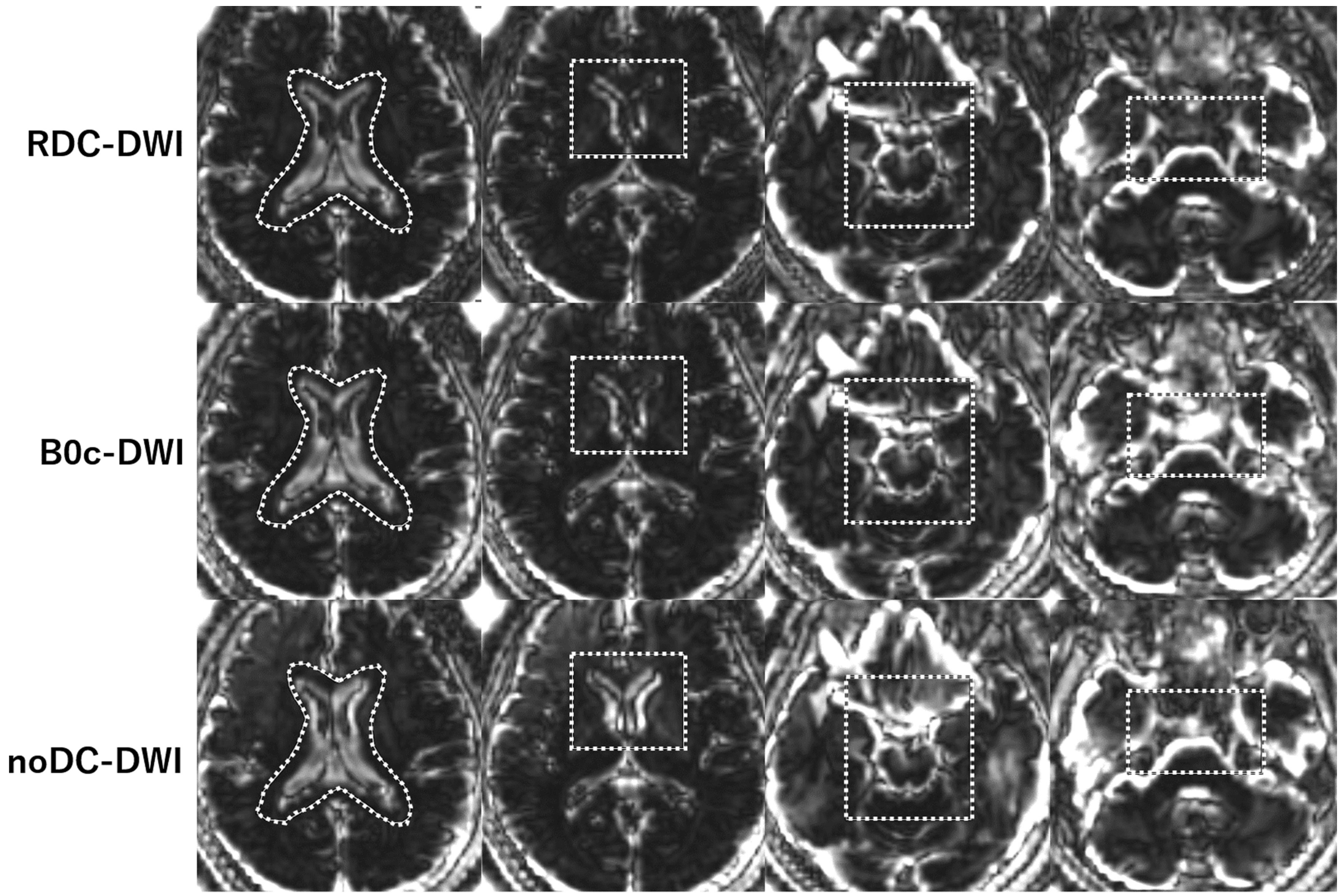


**Fig. 5** Representative $CV_{distortion}$ images and ROIs (dashed lines) in images of a female participant aged 67 years. From left to right, the images are at the level of the splenium of the corpus callosum, genu of the corpus callosum, optic chiasm, and middle cerebellar peduncle. At the level of the splenium of the corpus callosum, a polygonal ROI was drawn to cover the left and right lateral ventricles. At the level of the genu of the corpus callosum, a rectangular ROI was drawn to cover the anterior part of the lateral ventricles. At the level of the optic chiasm, a rectangular ROI was drawn to cover the pre-pontine cistern. At the level of the cerebellar peduncle, a rectangular ROI was drawn to cover the suprasellar area. Each ROI was first drawn on RDC-DWI and then copied to B0c-DWI and noDC-DWI. Usually, there was no misalignment. B0c, images with B0 correction only; $CV_{distortion}$, distortion image using coefficient of variation; DWI, diffusion-weighted imaging; noDC, images without distortion correction; RDC, reverse encoding distortion correction.

orientations. In the phantom study, distortion was the least in RDC-DWI followed by B0c-DWI and noDC-DWI. In the volunteer scan, in all location except for middle cerebellar peduncle, distortion was the least in RDC-DWI followed by B0c-DWI and noDC-DWI. This result shows that generally both in the phantom and in the volunteers, RDC-DWI performed better than B0c. The difference between RDC and B0c is that a pair of DWI is used to calculate shift maps (RDC) or not (B0c). This may mean that "eddy-current effects" seen in the DWI is corrected by applying the same technique to correct distortion in the b0 image. The advantage of using DWI for distortion correction was also reported by other researchers. For example, Irfanoglu et al.[10] showed that the quality of the DTI color map can be improved compared with the method using the b0 image alone. The difference in the method is that they used additional anatomical information seen in the white matter in DWI. The scan time for B0c-DWI is almost a half of that for RDC-DWI because of the number of the acquired b1000 images. However, our result showed that B0c suffers from larger distortion compared with RDC-DWI. Although RDC-DWI requires longer scan time, advantage in the distortion correction was significant.

### *Limitations*

There are several limitations in this study. First, RDC requires two pairs of images in the reversed phase-encoding direction. In the clinical setting, however, DWI might be obtained with only one average. To overcome this limitation, a deep-learning-based approach[5] that does not require paired

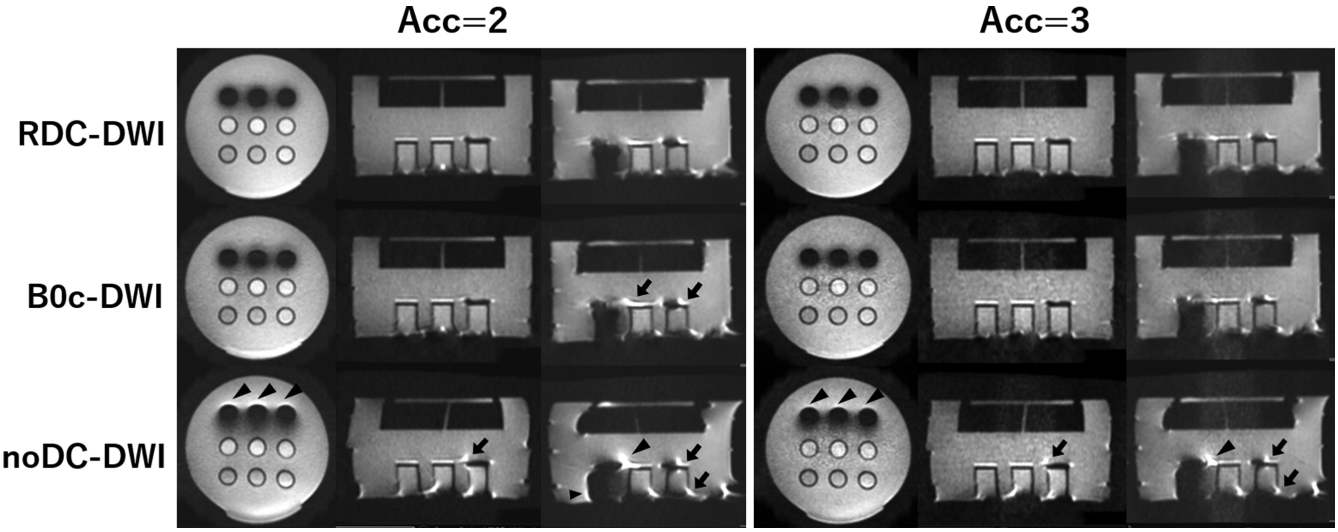


**Fig. 6** Representative slices of the phantom in the axial, coronal, and sagittal planes for each of RDC-DWI, B0c-DWI, and noDC-DWI with acceleration factors of 2 (left) and 3 (right). The arrows indicate susceptibility artifact, which is prominent around the empty tubes (arrowheads). Distortion of shapes within the phantom is most prominent in noDC-DWI (for both Acc 2 and 3) compared with B0c-DWI and RDC-DWI, and is less for Acc 3 than Acc 2. B0c, images with B0 correction only; DWI, diffusion-weighted imaging; noDC, images without distortion correction; RDC, reverse encoding distortion correction.

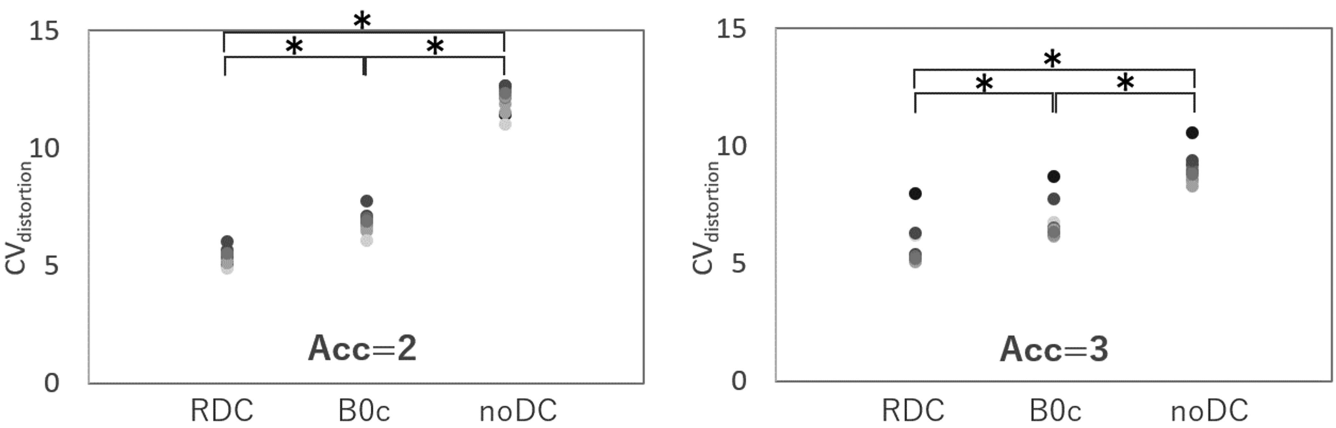


**Fig. 7** $CV_{distortion}$ in circular ROIs covering all nine tubular areas in RDC-DWI, B0c-DWI, and noDC-DWI for acceleration factors of 2 and 3. Asterisks (*) indicate significant difference ($P < 0.05$). For both Acc 2 and 3, $CV_{distortion}$ was significantly less in RDC-DWI than in B0c-DWI and noDC-DWI. Similarly, $CV_{distortion}$ was significantly less in B0c-DWI than in noDC-DWI. B0c, images with B0 correction only; $CV_{distortion}$, distortion image using coefficient of variation; DWI, diffusion-weighted imaging; noDC, images without distortion correction; RDC, reverse encoding distortion correction.

images has recently been proposed for removing distortion. Second, as the present participants were all healthy, we were unable to evaluate the detectability of abnormal lesions. Third, the effect of metal objects such as surgical clips was not evaluated. We assume that RDC-DWI would be effective to some extent against distortion caused by metal implants; however, further clinical studies are required to evaluate its efficacy. Fourth, we did not use a dedicated diffusion phantom. It is known that ADC values are sensitive to thermal control issues.[18] Nevertheless, we observed no significant change in ADC values during imaging of the phantom used in the present study. Fifth, the metric of $CV_{distortion}$ used in this study do not directly measure the degree of image distortion itself. Although we consider it as a metric for distortion, this metric only measures similarity in the degree of distortion seen in the three (orthogonal) scan orientations.

## Conclusion

Distortion was less in RDC-DWI than in B0c-DWI and noDC-DWI in both the phantom study and in healthy

**Table 2** Mean ADC values of 25 scans, intra-scan $\%CV_{ADC}$, inter-scan $\%CV_{ADC}$ were shown for RDC-DWI (a), B0c-DWI (b), and noDC-DWI (c)

**(a) RDC-DWI**

| scan \ day | 1 | 2 | 3 | 4 | 5 | $\%CV_{ADC}$ (inter-scan) |
|---|---|---|---|---|---|---|
| 1 | 0.00121 | 0.00123 | 0.00124 | 0.00119 | 0.00129 | 2.76 |
| 2 | 0.00121 | 0.00122 | 0.00123 | 0.00118 | 0.00127 | 2.43 |
| 3 | 0.00122 | 0.00122 | 0.00124 | 0.00118 | 0.00128 | 2.55 |
| 4 | 0.00122 | 0.00122 | 0.00125 | 0.00119 | 0.00128 | 2.40 |
| 5 | 0.00121 | 0.00124 | 0.00125 | 0.00119 | 0.00126 | 2.17 |
| $\%CV_{ADC}$ (intra-scan) | 0.30 | 0.48 | 0.54 | 0.39 | 0.64 | |

**(b) B0c-DWI**

| scan \ day | 1 | 2 | 3 | 4 | 5 | $\%CV_{ADC}$ (inter-scan) |
|---|---|---|---|---|---|---|
| 1 | 0.00123 | 0.00125 | 0.00126 | 0.00126 | 0.00133 | 2.70 |
| 2 | 0.00123 | 0.00125 | 0.00124 | 0.00124 | 0.00132 | 2.52 |
| 3 | 0.00124 | 0.00125 | 0.00127 | 0.00125 | 0.00132 | 2.05 |
| 4 | 0.00124 | 0.00124 | 0.00127 | 0.00126 | 0.00132 | 2.19 |
| 5 | 0.00124 | 0.00126 | 0.00128 | 0.00126 | 0.00131 | 1.79 |
| $\%CV_{ADC}$ (intra-scan) | 0.32 | 0.44 | 0.97 | 0.55 | 0.59 | |

**(c) noDC-DWI**

| scan \ day | 1 | 2 | 3 | 4 | 5 | $\%CV_{ADC}$ (inter-scan) |
|---|---|---|---|---|---|---|
| 1 | 0.00123 | 0.00123 | 0.00126 | 0.00122 | 0.00132 | 2.99 |
| 2 | 0.00124 | 0.00123 | 0.00125 | 0.00121 | 0.00129 | 1.93 |
| 3 | 0.00124 | 0.00125 | 0.00124 | 0.00124 | 0.00131 | 2.12 |
| 4 | 0.00122 | 0.00124 | 0.00127 | 0.00125 | 0.00129 | 1.84 |
| 5 | 0.00123 | 0.00125 | 0.00129 | 0.00121 | 0.00129 | 2.59 |
| $\%CV_{ADC}$ (intra-scan) | 0.47 | 0.63 | 1.24 | 1.30 | 1.03 | |

ADC, apparent diffusion coefficient; B0c, images with B0 correction only; DWI, diffusion-weighted imaging; noDC, images without distortion correction; RDC, reverse encoding distortion correction.

volunteers. Although ADC values were significantly lower (by 1.91%) in RDC-DWI than in noDC-DWI in the phantom, the result was comparable with inter-scan variability (%CV = 1.79%–2.99%).

## Acknowledgments

The authors would like to thank Yuichiro Sano and Nobuyasu Ichinose for fruitful discussions and feedback regarding the manuscript.

## Conflicts of Interest

Following authors are members of an industry-academia joint course between Kyoto University and Canon Medical Systems Corporation: Tsuneo Saga, MD, PhD; Kanae Kawai Miyake, MD, PhD; Koji Fujimoto, MD, PhD; and Hitomi Numamoto, RT. Rimika Imai and Hiroki Kondo MS are employees of Canon Medical Systems Corporation. The remaining authors have no conflicts of interest.

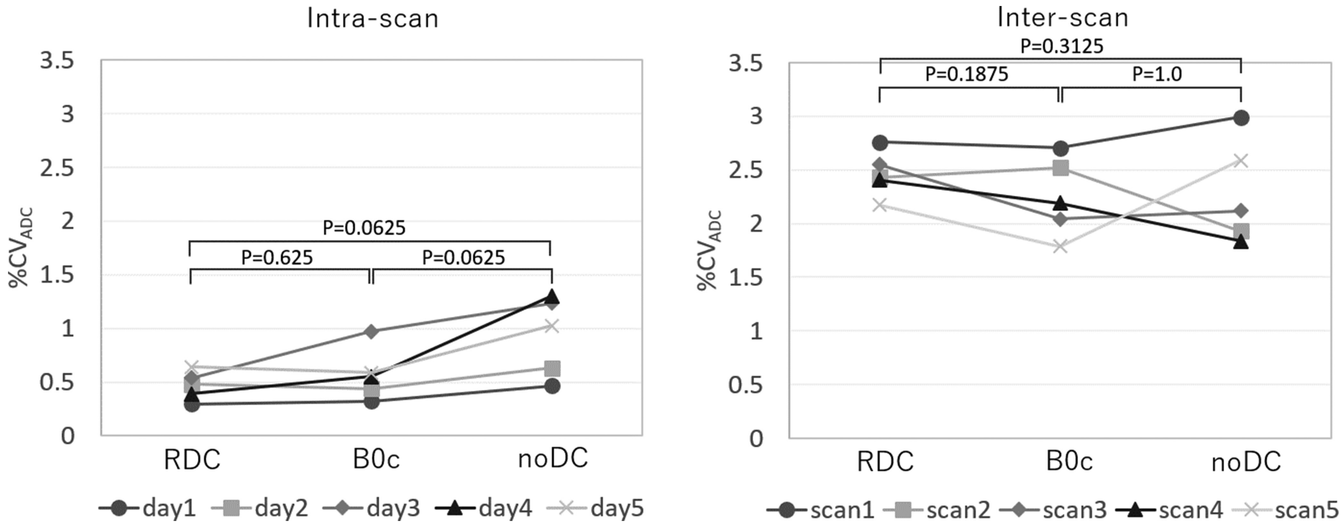


**Fig. 8** Intra-scan %CV$_{ADC}$ (left) and inter-scan %CV$_{ADC}$ (right) for the three different methods (RDC, B0c, and noDC). There was no significant difference in %CV$_{ADC}$ among RDC-DWI, B0c-DWI, and noDC-DWI in terms of intra-scan %CV$_{ADC}$ or inter-scan %CV$_{ADC}$. ADC, apparent diffusion coefficient; B0c, images with B0 correction only; DWI, diffusion-weighted imaging; noDC, images without distortion correction; RDC, reverse encoding distortion correction.

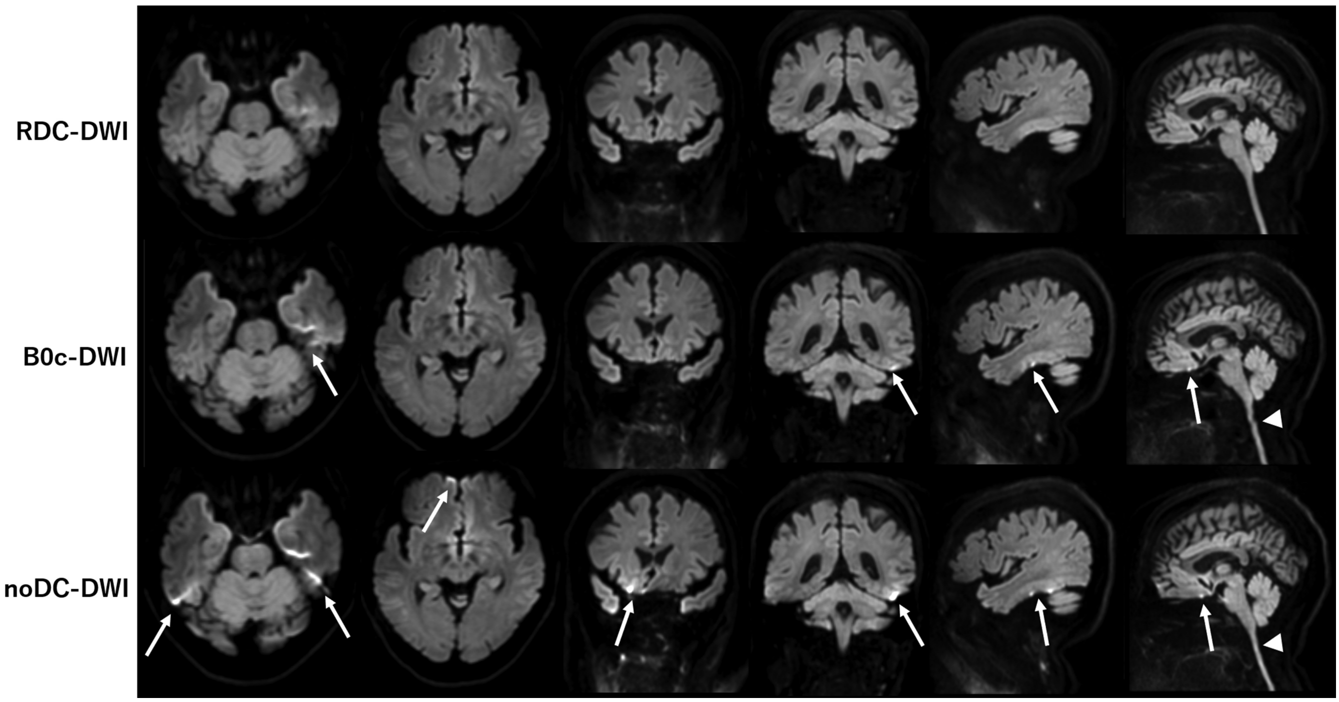


**Fig. 9** Representative axial, coronal, and sagittal DWI (b = 1000) of a female participant aged 70 years. The upper, middle, and bottom rows show RDC-DWI, B0c-DWI, and noDC-DWI, respectively. In the axial images, distortion is seen in the area adjacent to the left sphenoid sinus and is more prominent in B0c-DWI (arrow) than in noDC-DWI (arrow). Distortion seen in the insula and left lower temporal lobe in coronal B0c-DWI is more prominent in noDC-DWI. In sagittal B0c-DWI and noDC-DWI, areas of high signal intensity are seen in the right temporal lobe and in the suprasellar region, and B0c-DWI and noDC-DWI show signal inhomogeneity in the spinal cord (arrowheads). B0c, images with B0 correction only; DWI, diffusion-weighted imaging; noDC, images without distortion correction; RDC, reverse encoding distortion correction.

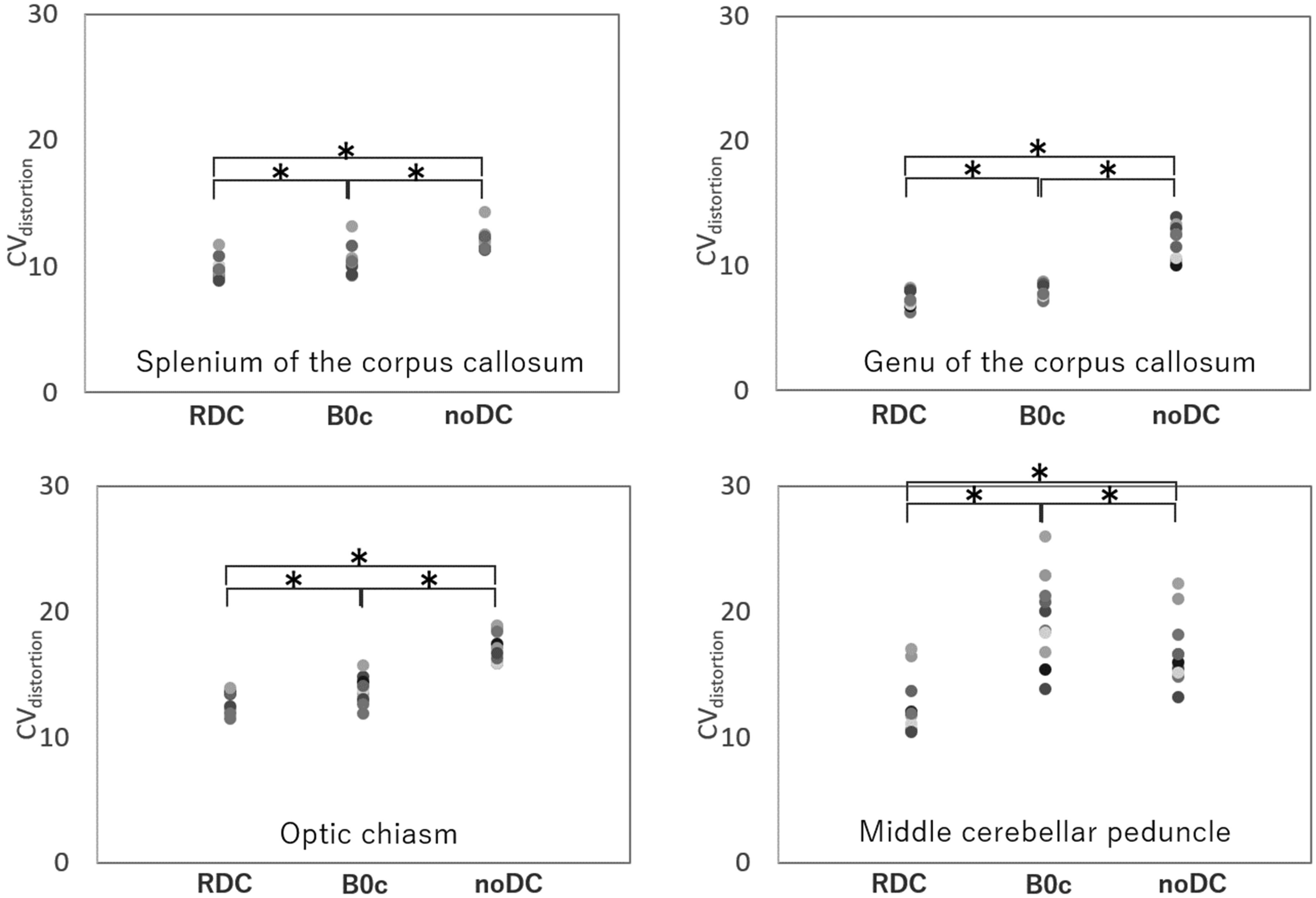


**Fig. 10** $CV_{distortion}$ values for the three different methods (RDC, B0c, and noDC) at four different levels of the brain (splenium of the corpus callosum, genu of the corpus callosum, optic chiasm, and middle cerebellar peduncle). Asterisks (*) indicate significant difference ($P < 0.05$). At all locations, $CV_{distortion}$ was significantly less for RDC than for B0c and noDC. Except for the middle cerebellar peduncle, $CV_{distortion}$ was significantly less for B0c than for noDC, and $CV_{distortion}$ was significantly less for noDC than for B0c. B0c, images with B0 correction only; $CV_{distortion}$, distortion image using coefficient of variation; noDC, images without distortion correction; RDC, reverse encoding distortion correction.

## Supplementary Materials

(1) For RDC-DWI, 24 b1000 images (i.e. NEX4, three MPG directions, forward and reverse phase encoding directions) were used for each slice to obtain six b1000 images by averaging over the same MPG directions and the same phase encoding directions. These six b1000 images (i.e. three MPG directions, forward and reverse phase encoding directions) were used to obtain three shift maps (B0 + Eddy) and six distortion corrected b1000 images. For each MPG direction, b1000 images were averaged to obtain three b1000 images. Finally, these three b1000 images were averaged to obtain one b1000 image (isoDWI=RDC-DWI).

(2) For B0c-DWI, 12 b1000 images (i.e. NEX4, three MPG directions, forward phase encoding directions) were used for each slice to obtain three b1000 images by averaging over the same MPG directions. Distortion in these three b1000 images (i.e. three MPG directions, forward phase encoding directions) was corrected by using a Shift map (B0) to obtain three distortion-corrected b1000 images. These three b1000 images were averaged to obtain one b1000 image (isoDWI=B0c-DWI).

(3) For noDC-DWI, 12 b1000 images (i.e. NEX4, three MPG directions, forward phase encoding directions) were used for each slice to obtain three b1000 images by averaging over the same MPG directions. These three b1000 images were averaged to obtain one b1000 image (isoDWI=noDC-DWI). B0c, images with B0 correction only; DWI, diffusion-weighted imaging; MPG, motion probing gradient; noDC, images without distortion correction; RDC, reverse encoding distortion correction.

## References

1. Morelli JN, Runge VM, Ai F, et al. An image-based approach to understanding the physics of MR artifacts. *Radiographics* 2011; 31:849–866.

2. Jezzard P, Balaban RS. Correction for geometric distortion in echo planar images from B0 field variations. *Magn Reson Med* 1995; 34:65–73.
3. Studholme C, Constable RT, Duncan JS. Accurate alignment of functional EPI data to anatomical MRI using a physics-based distortion model. *IEEE Trans Med Imaging* 2000; 19:1115–1127.
4. Andersson JL, Skare S, Ashburner J. How to correct susceptibility distortions in spin-echo echo-planar images: application to diffusion tensor imaging. *Neuroimage* 2003; 20:870–888.
5. Schilling KG, Blaber J, Hansen C, et al. Distortion correction of diffusion weighted MRI without reverse phase-encoding scans or field-maps. *PLoS One* 2020; 15:e0236418.
6. Chang H, Fitzpatrick JM. A technique for accurate magnetic resonance imaging in the presence of field inhomogeneities. *IEEE Trans Med Imaging* 1992; 11:319–329.
7. Bowtell R, McIntyre DJO, Commandre M-J, Glover PM, Mansfield P. Correction of geometric distortion in echo planar images. Proceedings of the International Society for Magnetic Resonance in Medicine, San Francisco, 1994; 411.
8. Andersson JL, Skare S. A model-based method for retrospective correction of geometric distortions in diffusion-weighted EPI. *Neuroimage* 2002; 16:177–199.
9. Hedouin R, Commowick O, Bannier E, et al. Block-matching distortion correction of echo-planar images with opposite phase encoding directions. *IEEE Trans Med Imaging* 2017; 36:1106–1115.
10. Irfanoglu MO, Modi P, Nayak A, Hutchinson EB, Sarlls J, Pierpaoli C. DR-BUDDI (Diffeomorphic Registration for Blip-Up blip-Down Diffusion Imaging) method for correcting echo planar imaging distortions. *Neuroimage* 2015; 106:284–299.
11. Holland D, Kuperman JM, Dale AM. Efficient correction of inhomogeneous static magnetic field-induced distortion in Echo Planar Imaging. *Neuroimage* 2010; 50:175–183.
12. Andersson JLR, Sotiropoulos SN. An integrated approach to correction for off-resonance effects and subject movement in diffusion MR imaging. *Neuroimage* 2016; 125:1063–1078.
13. Morgan PS, Bowtell RW, McIntyre DJ, Worthington BS. Correction of spatial distortion in EPI due to inhomogeneous static magnetic fields using the reversed gradient method. *J Magn Reson Imaging* 2004; 19:499–507.
14. Skare S, Andersson JL. Correction of MR image distortions induced by metallic objects using a 3D cubic B-spline basis set: application to stereotactic surgical planning. *Magn Reson Med* 2005; 54:169–181.
15. Embleton KV, Haroon HA, Morris DM, Ralph MA, Parker GJ. Distortion correction for diffusion-weighted MRI tractography and fMRI in the temporal lobes. *Hum Brain Mapp* 2010; 31:1570–1587.
16. Irfanoglu MO, Sarlls J, Nayak A, Pierpaoli C. Evaluating corrections for Eddy-currents and other EPI distortions in diffusion MRI: methodology and a dataset for benchmarking. *Magn Reson Med* 2019; 81:2774–2787.
17. Sjöholm T, Kullberg J, Strand R, Engström M, Ahlström H, Malmberg F. Improved geometric accuracy of whole body diffusion-weighted imaging at 1.5T and 3T using reverse polarity gradients. *Sci Rep* 2022; 12:11605.
18. Moreau B, Iannessi A, Hoog C, Beaumont H. How reliable are ADC measurements? A phantom and clinical study of cervical lymph nodes. *Eur Radiol* 2018; 28:3362–3371.
19. Miquel ME, Scott AD, Macdougall ND, Boubertakh R, Bharwani N, Rockall AG. In vitro and in vivo repeatability of abdominal diffusion-weighted MRI. *Br J Radiol* 2012; 85:1507–1512.
20. Wang Y, Tadimalla S, Rai R, et al. Quantitative MRI: Defining repeatability, reproducibility and accuracy for prostate cancer imaging biomarker development. *Magn Reson Imaging* 2021; 77:169–179.